Luminescence-center-mediated excitation as the dominant Er sensitization mechanism in Er-doped silicon-rich SiO_2 films

Oleksandr Savchyn,* Forrest R. Ruhge, and Pieter G. Kik†
CREOL, The College of Optics and Photonics, University of Central Florida, 4000 Central Florida Boulevard, Orlando, Florida 32816, USA

Ravi M. Todi,‡,§ Kevin R. Coffey,‖,‡,† Haritha Nukala, and Helge Heinrich†
Advanced Materials Processing and Analysis Center (AMPAC), University of Central Florida, 4000 Central Florida Boulevard, Orlando, Florida 32816, USA

(Received 8 August 2007; published 15 November 2007)

The structural and optical properties of erbium-doped silicon-rich silica samples containing 12 at. % of excess silicon and 0.63 at. % of erbium are studied as a function of annealing temperature in the range 600–1200 °C. Indirect excitation of Er^{3+} ions is shown to be present for all annealing temperatures, including annealing temperatures well below 1000 °C for which no silicon nanocrystals are observed. Two distinct efficient ($\eta_{tr}>60\%$) transfer mechanisms responsible for Er^{3+} excitation are identified: a fast transfer process ($\tau_{tr}<80$ ns) involving isolated luminescence centers (LCs), and a slow transfer process ($\tau_{tr}\sim 4-100$ μs) involving excitation by quantum confined excitons inside Si nanocrystals. The LC-mediated excitation is shown to be the dominant excitation mechanism for all annealing temperatures. The presence of a LC-mediated excitation process is deduced from the observation of an annealing-temperature-independent Er^{3+} excitation rate, a strong similarity between the LC and Er^{3+} excitation spectra, as well as an excellent correspondence between the observed LC-related emission intensity and the derived Er^{3+} excitation density for annealing temperatures in the range of 600–1000 °C. The proposed interpretation provides an alternative explanation for several observations existing in the literature.

DOI: 10.1103/PhysRevB.76.195419 PACS number(s): 78.67.Bf, 71.35.Gg, 71.55.−i, 76.30.Kg

I. INTRODUCTION

In recent years there has been tremendous interest in the use of erbium in silicon based photonics.[1–7] Erbium is a well known optical dopant that can provide optical gain at 1.5 μm when incorporated into glass hosts. The gain is due to the $^4I_{13/2}\rightarrow{}^4I_{15/2}$ transition in the incompletely filled $4f$ shell of the Er^{3+} ion. The Er^{3+} ion exhibits several sharp absorption lines with a typical absorption cross section on the order of $\sim 10^{-20}-10^{-21}$ cm^2.[8] For this reason, high power resonant excitation is generally needed in order to reach population inversion and gain. This problem can be overcome by the incorporation of sensitizers into the host material, which exhibit a high absorption cross section and efficient energy transfer to the Er^{3+} ions.[9] Silicon nanocrystals have been considered as a possible optical sensitizer for Er^{3+} excitation since the first publications on indirect Er^{3+} excitation in several SiO_2 based materials. After the initial observations of indirect Er^{3+} excitation in partly oxidized porous silicon[10] and in oxygen-doped silicon,[11] convincing evidence for Er^{3+} excitation via quantum confined excitons in silicon nanocrystals in SiO_2 was found by Fujii *et al.*[12] In particular, a clear anticorrelation was observed between the intensity of a Si-nanocrystal-related emission band at ~800 nm and the Er^{3+} photoluminescence at 1535 nm. Additionally, the Er^{3+} excitation spectrum was found to be continuous, rather than exhibiting the sharp absorption lines associated with Er^{3+} intra-$4f$ transitions. The large absorption cross section of Si nanocrystals makes this an interesting material system with the potential of providing absorption cross sections in the range $\sim 10^{-18}-10^{-14}$ cm^2 for excitation energies between 1.5 and 3.5 eV.[13] This represents an increase of the Er^{3+} effective cross section by 3–6 orders of magnitude,[14–18] which opens the possibility of using low cost broadband light emitting diodes (LEDs) rather than diode lasers as pump sources for achieving gain. Since the initial observations of Si nanocrystal sensitized Er^{3+} excitation, Er^{3+}-related gain has been demonstrated in Er-doped Si-rich SiO_2 both under LED[19] and laser excitation.[19–21]

Despite the extensive amount of research on the topic, several important challenges and questions remain. An important practical challenge is the existence of confined carrier absorption, in which a quantum confined exciton can absorb sub-band-gap radiation with a cross section far exceeding the emission cross section of Er^{3+} at 1535 nm.[1,20,22,23] The magnitude of this effect depends on the lifetime of the excitons, and decreases with a decreasing nanocrystal-erbium transfer time. Work by Fujii *et al.*[24] revealed that while a slow transfer process exists ($\tau_{tr}\sim 1-70$ μs), the dominant energy transfer process occurs on a much faster time scale ($\tau_{tr}<100$ ns). The presence of these two processes is ascribed to energy transfer at different nanocrystal-erbium separations.[25] Further understanding of the origin of the fast transfer process is needed to minimize the effect of confined carrier absorption. A second unresolved issue involves the number of excitable Er^{3+} ions per nanocrystal, which affects the maximum gain that can be achieved in a Si-sensitized gain medium. Conflicting results exist in the literature, with some studies indicating that a Si nanocrystal can excite only 1–2 Er^{3+} ions based on lifetime measurements,[16,26] while other studies show that as many as ~20 Er^{3+} ions can be excited by a single nanocrystal by comparing photoluminescence in-

tensities observed under continuous wave and pulsed excitations.[18] A third issue involves the relatively small contribution of resonant Er^{3+} excitation. Resonant excitation would introduce dips in the nanocrystal photoluminescence spectrum due to energy transfer selectively from nanocrystals with an emission energy corresponding to an Er^{3+} transition. However, the incorporation of Er in Si-nanocrystal-doped SiO_2 generally leads to an overall intensity decrease across the entire nanocrystal spectrum, while only very minor dips have been observed at the location of Er^{3+}-related absorption bands at cryogenic temperatures.[27,28] This indicates that most of the energy transfer occurs nonresonantly. A fourth issue involves the observed independent behavior of the nanocrystal photoluminescence intensity and the Er^{3+} photoluminescence intensity in temperature dependent studies,[26,29] which has been explained by the existence of fast energy transfer. However, subsequent studies revealed that in many samples, the energy transfer to Er^{3+} at room temperature takes place on a time scale of tens of microseconds, posing a challenge to this explanation. A final issue is the relatively recent observation of indirect Er^{3+} excitation in Si-doped SiO_2 annealed at temperatures below the onset of the nanocrystal formation.[30–36]

In the present study, the structural properties and the room temperature photoluminescence behavior of Er-doped Si-rich SiO_2 were studied as a function of annealing temperature in the range 600–1200 °C. On the basis of the experimental results, we argue that luminescence centers (LCs) associated with excess-silicon-related electronic defects are responsible for most of the indirect Er^{3+} excitation at all annealing temperatures, with a small contribution due to nanocrystal-mediated Er^{3+} excitation in samples annealed at $T_{ann} \geqslant 1000$ °C. We show that the coexistence of LC-mediated and nanocrystal-mediated excitations can clarify several observations present in the literature.

II. EXPERIMENTAL TECHNIQUES

Samples were prepared using a multigun magnetron sputter deposition system (AJA International, Inc., ATC 2200-V). Silicon- and erbium-doped SiO_2 films were deposited onto P-doped silicon wafers (100) with a resistivity of 3–7 Ω cm by cosputtering from Si, SiO_2, and SiO_2:Er_2O_3 targets. The Er concentration in the mixed SiO_2:Er_2O_3 target was 1.8 at %. Depositions were conducted at room temperature in an Ar background pressure of 4 mTorr. The sample composition and thickness were verified using a Rutherford backscattering spectrometry (RBS) system (General IONIX 1.7 MU Tandetron), and RUMP software[37] was used to fit the recorded RBS spectra. Three types of samples were prepared: samples containing both excess Si (12 at %) and Er (0.63 at %), labeled "XSE" ("excess silicon and erbium"), and two types of reference samples: samples containing excess Si (11.5 at %) and no Er, labeled "XSO" ("excess silicon only"), and samples containing Er (0.49 at %) and no excess silicon, labeled "EO" ("erbium only"). The film thickness varied from sample to sample, and was found to be 92±20 nm. The samples were subsequently annealed for 100 s in flowing N_2 [flow rate of 3 SLPM (SLPM denotes standard liters per minute)] at ambient pressure using a rapid thermal processor (Modular Process Technology Corp., RTP-600S) at temperatures in the range of 600–1200 °C. The samples were then passivated at a temperature of 500 °C for 30 min in flowing forming gas [N_2:H_2=95%:5%, flow rate of 65 SCCM (SCCM denotes standard cubic centimeter per minute at STP)] in a tube furnace (Lindberg, 58114) and were allowed to cool down to room temperature under continued forming gas flow for 10 min. Microstructural characterization of the annealed samples was performed using a transmission electron microscope (FEI Technai F30). Sample cross sections for transmission electron microscopy measurements were prepared by focused ion-beam milling. Room temperature photoluminescence measurements were taken using the 351 nm emission line of a Kr-ion laser (Spectra-Physics, BeamLok 2060) as the excitation source. The pump power used was 0.66 mW, and the spot size on the sample was ~1 mm^2 unless specified otherwise. The photoluminescence signal was focused into the entrance slits of a single monochromator (Acton, 2300i), and a long pass filter with a cutoff wavelength of 400 nm was placed in front of the entrance slits to block the laser light. Visible photoluminescence spectra were recorded using a thermoelectrically cooled charge coupled device camera (Andor, DU401-BR-DD). Near-infrared spectra were obtained using a liquid-nitrogen-cooled Ge detector (Applied Detector Corp., 403S) in combination with standard lock-in techniques. All spectra were corrected for the system response, and intensities were corrected for variations in film thickness. For time-dependent photoluminescence measurements, the pump beam was modulated using an acousto-optic modulator (NEOS Technologies, 38210-6AS). Photoluminescence traces were obtained using photomultiplier tubes (Hamamatsu R4330-02 for the visible region and Hamamatsu 5509-73 for the near-infrared region) in combination with a multichannel scaler (Stanford Research Systems, SR430). The spectral resolution in all photoluminescence measurements was ~15 nm. The time resolution in all measurements presented in this study was better than 80 ns. Photoluminescence excitation spectra were taken using multiple Kr-ion emission lines at a pump power of ~1 mW and a spot size of ~3 mm^2.

III. RESULTS AND DISCUSSION

A. Microstructure

The microstructure of the samples was studied using cross sectional transmission electron microscopy (TEM). Figure 1(a) shows the bright field cross sectional TEM image of an as-deposited XSE sample. The inset shows a magnified view of the area marked by the dashed white square. No clear phase separation is observed, and no lattice fringes could be detected. For the sample annealed at 600 °C [Fig. 1(b)], a similar sample structure is observed, although a slight intensity contrast appears to be present at length scales on the order of ~10 nm. Again no lattice fringes are observed. The electron diffraction pattern shows bright spots due to the diffraction from the substrate. No diffraction spots related to randomly oriented nanocrystals are observed [Fig. 1(c)]. For an annealing temperature of 1000 °C [Fig. 1(d)], clearly

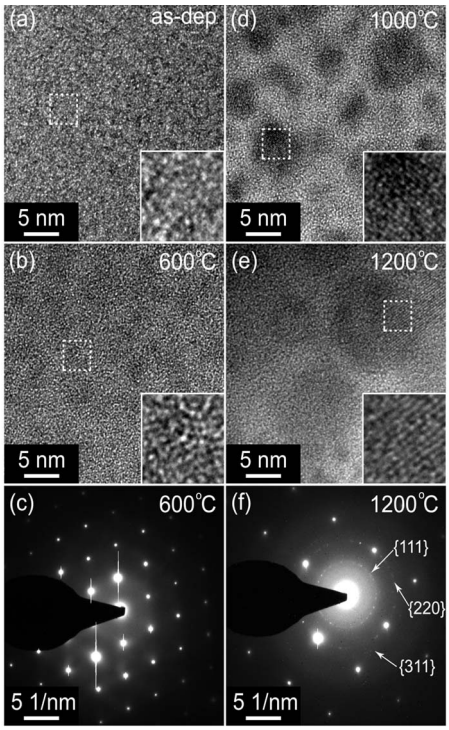

FIG. 1. High-resolution bright field TEM images of Er-doped Si-rich SiO_2 samples (a) as-deposited, (b) annealed at 600 °C, (d) annealed at 1000 °C, and (e) annealed at 1200 °C. Electron diffraction patterns for (c) the sample annealed at 600 °C and (f) the sample annealed at 1200 °C. The insets show a magnified view of the area indicated by the dashed squares.

separated dark regions with typical diameters in the range 5–10 nm are observed, indicating the onset of nanocluster formation. In some of these dark regions, lattice fringes are clearly observed, indicating that at least some of the observed clusters are crystalline. Samples annealed at 1200 °C [Fig. 1(e)] show larger cluster sizes and extended regions with clear lattice fringes, indicating continued nanocrystal growth. Figure 1(f) shows the electron diffraction pattern obtained from a sample annealed at 1200 °C. An array of bright diffraction spots is seen due to diffraction from the substrate imaged along [001]; additionally, faint rings consisting of individual diffraction spots are observed. The latter are caused by diffraction from randomly oriented crystallites in the SiO_2 matrix. Rings corresponding to the diffraction from {111}, {220}, and {311} lattice planes of Si nanocrystals are clearly seen. Note that one of the diffraction rings crosses a Si substrate diffraction spot, indicating that the crystallites indeed have a lattice spacing corresponding to that of silicon.

B. Photoluminescence spectra

Figure 2 (top) shows the photoluminescence (PL) spectra obtained from samples containing excess silicon only (XSO) annealed at temperatures in the range of 600–1200 °C. A broad emission band peaking at wavelengths near 500 nm is observed for all annealing temperatures, and is stronger for the lower annealing temperatures used. Note that this band is observed at annealing temperatures (T_{ann}) well below those

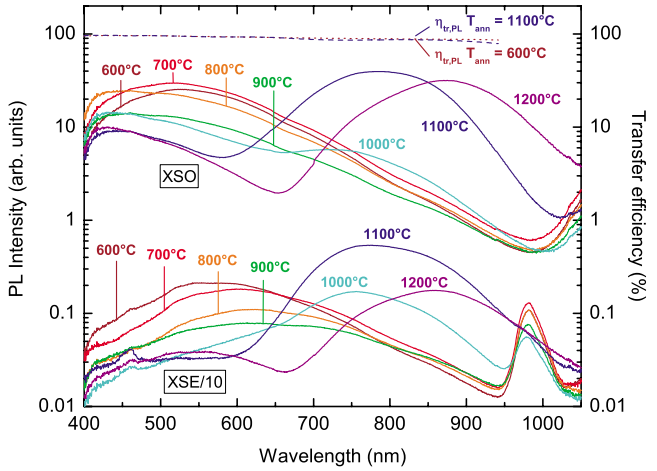

FIG. 2. (Color online) Photoluminescence spectra of passivated Si-rich SiO_2 films with (XSE) and without (XSO) erbium, annealed at temperatures in the range 600–1200 °C. The inferred spectral dependence of the transfer efficiency is included for annealing temperatures of 600 and 1100 °C.

required for the onset of silicon nanocrystal nucleation and growth, which has been shown to occur at $T_{ann} > 1000$ °C.[38] Photoluminescence decay measurements at an emission wavelength of 500 nm (not shown) reveal a resolution limited decay, indicating that the decay time of this feature is less than 80 ns. This type of fast short-wavelength emission has been observed in several studies, and is considered to be caused by LCs associated with oxygen deficiencies that are formed as a result of the nonstoichiometric composition of Si-rich SiO_2.[39–42] Note that as the annealing temperature is increased, the intensity of this band decreases, possibly due to the gradual removal of the luminescence centers upon annealing. Contrary to previously published results on ion-beam-induced defects in SiO_2,[43] hydrogen passivation was found to result in an intensity increase of the LC-related band by a factor of ~2 for all samples (not shown). The reason for this different behavior of the LC photoluminescence upon passivation is not fully understood at this time; however, it seems likely that different LCs are formed depending on the sample preparation method. At annealing temperatures above 900 °C, a broad emission band peaking between 800 and 900 nm is observed in XSO samples. Photoluminescence decay measurements of this band at an emission wavelength of 900 nm reveal lifetimes in the range of 12–142 μs for samples annealed at temperatures in the range of 1000–1200 °C. Such slow emission at these wavelengths is commonly attributed to radiative exciton recombination in relatively large silicon nanocrystals (NCs) ($d > 4$ nm) (Refs. 44–46) formed in the Si-rich SiO_2 matrix upon annealing. Note that the observed emission wavelength is too long to be attributed to the recombination of electrons and holes at Si=O surface states as discussed in Refs. 45 and 47.

Figure 2 also includes emission spectra from samples containing excess Si and Er (XSE). Note that the signal from these samples has been divided by a factor of 10 for clarity. Both the short-wavelength LC-related emission and the NC-

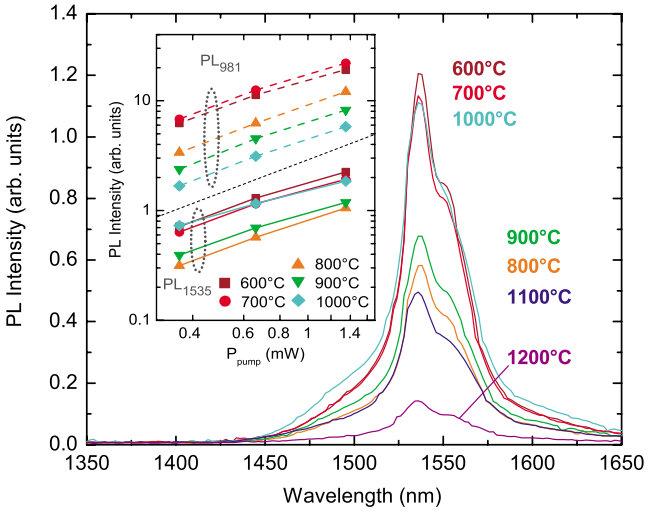

FIG. 3. (Color online) Near-infrared photoluminescence spectra of passivated Er-doped Si-rich SiO_2 samples annealed at temperatures in the range 600–1200 °C. Inset: the Er^{3+}-related peak emission intensity at 981 and 1535 nm as a function of pump power. The dashed line indicates a linear dependence.

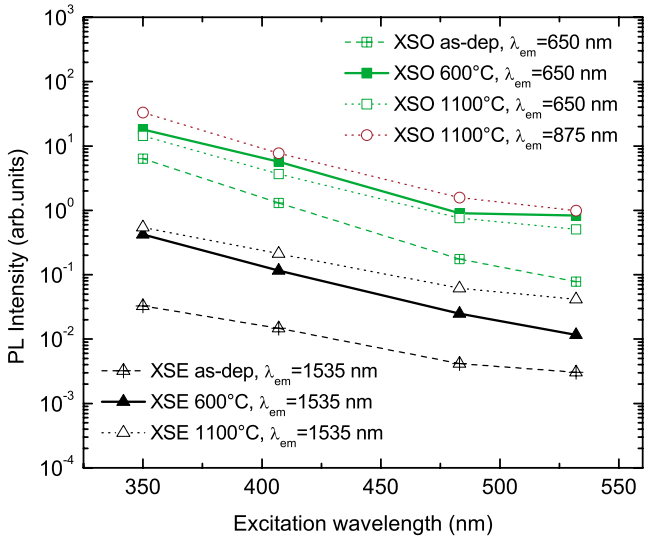

FIG. 4. (Color online) Photoluminescence excitation spectra of passivated Si-rich SiO_2 films with (XSE) and without (XSO) erbium for an as-deposited sample as well as samples annealed at 600 and at 1100 °C, measured at emission wavelengths predominantly corresponding to luminescence center emission (650 nm), Si nanocrystal emission (875 nm), and Er^{3+} emission (1535 nm).

related emission drop by approximately an order of magnitude in the presence of erbium for all annealing temperatures. This type of drop in the NC emission upon Er incorporation has been previously attributed to energy transfer from quantum confined excitons to erbium,[12] resulting in a reduced NC emission efficiency. Analogously, the reduced LC emission at short wavelengths suggests that the luminescence centers also interact with Er^{3+} ions on a time scale that is significantly faster than the lifetime of the LC emission observed in XSO samples of $\tau_{LC} < 80$ ns. The possibility of LC-mediated Er^{3+} excitation is discussed in more detail below.

In addition to the LC- and NC-related emission bands observed in Fig. 2, an Er^{3+}-related signal is observed at 981 nm for XSE samples, corresponding to the transition from the second excited state to the ground state of Er^{3+} ($^4I_{11/2} \rightarrow {}^4I_{15/2}$). Figure 3 shows the near-infrared spectra for the XSE samples under the same excitation conditions. A clear Er^{3+}-related emission spectrum peaking at 1535 nm is observed, corresponding to the transition from the first excited state to the ground state of Er^{3+} ($^4I_{13/2} \rightarrow {}^4I_{15/2}$). Neither of these Er^{3+}-related features were observed in XSO samples (i.e., in the samples not containing Er). Although the excitation wavelength of 351 nm used in the present experiments lies in the vicinity of an Er^{3+} absorption line at 355 nm ($^4I_{15/2} \rightarrow {}^2G_{7/2}$),[48,49] no Er^{3+}-related emission was detected at the same pump power in Er-doped SiO_2 (EO samples). This clearly indicates that the observed Er^{3+} PL in Figs. 2 and 3 is the result of indirect excitation.

The inset in Fig. 3 shows the pump power dependence of the background corrected 981 nm emission as well as the 1535 nm emission for samples annealed at different temperatures up to a pump power of 1.35 mW. For reference, a linear pump power dependence is indicated by the dashed line. Note that no Er^{3+}-related 981 nm emission could be resolved in samples annealed at $T_{ann} > 1000$ °C. Both Er^{3+}-related peaks exhibit approximately the same near-linear dependence for all annealing temperatures in this pump power range, indicating that the 981 nm emission is not caused by excited state absorption or cooperative upconversion. These observations demonstrate that a finite fraction of the Er^{3+} ions is excited into the $^4I_{11/2}$ level or into higher lying levels followed by nonradiative relaxation.

C. Evidence for luminescence-center-mediated excitation

Figure 4 shows the excitation spectra of the PL intensity at 650 nm (squares) and 875 nm (circles) from XSO samples, as well as the PL intensity at 1535 nm (triangles) from XSE samples. These emission wavelengths correspond to PL predominantly from the luminescence centers, the Si nanocrystals, and the Er^{3+} ions, respectively. Results for the as-deposited samples as well as the samples annealed at 600 and 1100 °C are shown. The PL intensity was corrected for the system response at the detection wavelength, and normalized to the incident photon flux. For the sample annealed at 600 °C (solid lines), both the Er^{3+} emission and the LC emission intensities show a gradual increase as the excitation wavelength is decreased, increasing by more than a factor of 20 over this measurement range. The corresponding excitation spectra of the as-deposited unpassivated sample (dashed lines) are seen to exhibit a very similar spectral dependence. The gradual increase of the Er^{3+} emission intensity with decreasing wavelength is commonly attributed to Er^{3+} excitation by quantum confined excitons in Si NCs. This interpretation is indeed compelling, since the observed Er^{3+} excitation spectrum rather closely follows the expected Si absorption spectrum (not shown). However, no Si nanocrystals were observed in the TEM measurements of as-deposited samples and samples annealed at 600 °C, and no distinguish-

able NC-related emission is observed at $T_{ann}=600\ ^{\circ}C$ (see Fig. 2). The similarity between the Er^{3+} excitation spectrum and the LC excitation spectrum in these samples suggests that at these annealing temperatures, the erbium is excited via isolated luminescence states in the SiO_2 band gap or via (surface states on) undetectably small Si nanoclusters. The shape of the excitation spectrum suggests that these states either individually exhibit a broad absorption spectrum, or that the density of these states (or, more precisely, the joint density of states) increases as a function of increasing photon energy. In the sample annealed at 1100 °C (dotted lines), the Er^{3+} emission, the NC emission, and the LC emission all show a virtually identical increase in intensity as the excitation wavelength is decreased. The behavior of the Er^{3+} PL and the NC PL in these samples is similar to that observed in numerous other studies. The similarity of the NC and Er^{3+} excitation spectra in this sample could indicate that in samples annealed at 1100 °C, the Er^{3+} ions are excited via quantum confined excitons. However, due to the similarity of the excitation spectra of the NC band and the LC band, these data cannot provide information on the relative contribution of NC- and LC-mediated Er^{3+} excitations.

To further investigate the nature of the indirect Er^{3+} excitation in these samples, an extensive set of PL measurements was carried out on XSO and XSE samples annealed at different temperatures. The results of these measurements are summarized in Fig. 5. Unless stated otherwise, all the data were acquired using an excitation wavelength of 351 nm and an excitation power of 0.66 mW.

Figure 5(a) shows the measured photoluminescence peak intensity (I_{Er}, solid circles) as well as the $1/e$ lifetime ($\tau_{dec,Er}$, open circles) of the Er^{3+}-related emission at $\lambda=1535$ nm for XSE samples. The Er^{3+} peak intensity at 1535 nm exhibits a moderate drop as the annealing temperature is increased from 600 to 800 °C. This drop is followed by a brief gradual increase and, subsequently, a rather steep Er^{3+} PL decrease at $T_{ann}>1000\ ^{\circ}C$. Note that the location of the steep drop coincides with the temperature of the observed nanocrystal formation. The measured Er^{3+} decay traces all exhibited a small degree of multiexponentiality that is well described by a stretched exponential decay of the form $I_{Er}(t) \propto \exp[-(t/\tau_{dec,Er})^{\beta}]$ with a dispersion factor $\beta \approx 0.80 \pm 0.02$. The Er^{3+} lifetime is found to increase significantly as the annealing temperature is increased, which is generally attributed to the removal of defects, relaxation of bond angles, and reduction of bond length distortions that can cause nonradiative decay of Er^{3+}-related emission in SiO_2.[50,51]

Figure 5(b) shows the temperature dependence of the PL intensity at $\lambda_{em}=650$ nm, which is predominantly representative of the LC emission (open squares), and the intensity at $\lambda_{em}=900$ nm, which is predominantly representative of the NC emission intensity for $T_{ann} \geq 1000\ ^{\circ}C$ (open circles). The LC emission is seen to *decrease* by a factor ~10 over the shown temperature range, while the PL intensity at 900 nm is seen to *increase* rapidly as T_{ann} is increased beyond 900 °C due to the development of the strong NC-related PL band (see spectra in Fig. 2). In order to correlate the Er^{3+} emission with either the LC emission or the NC emission, we first derive the Er^{3+} excitation density $\rho_{exc,Er}$, defined as the number of Er^{3+} excitation events per second per unit volume.

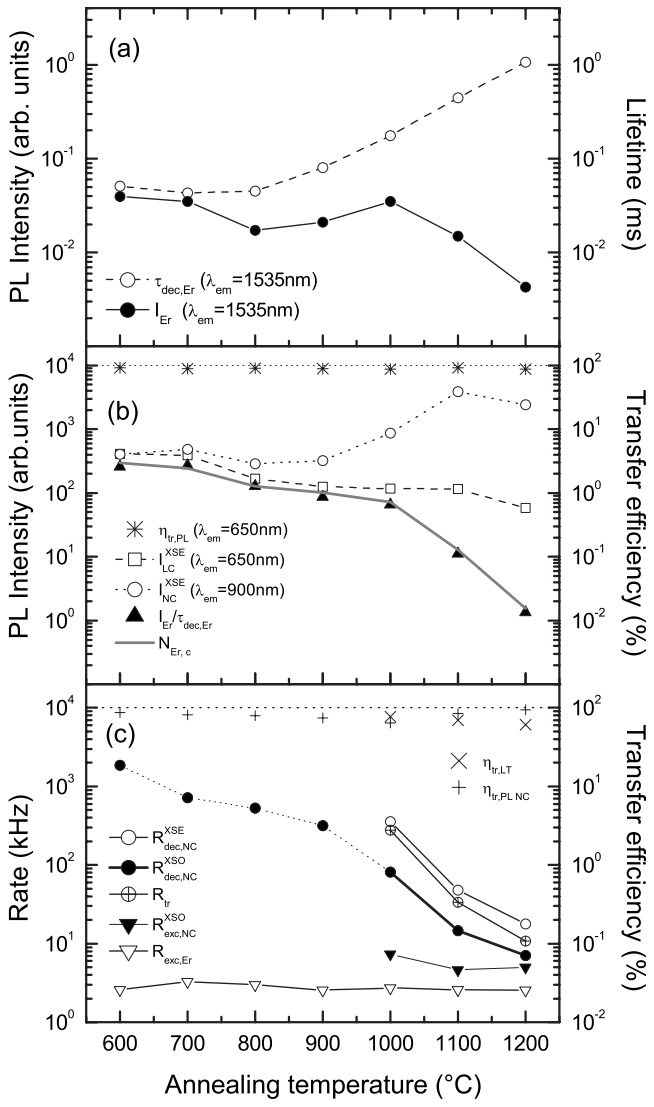

FIG. 5. Measured and deduced PL parameters of passivated Si-rich SiO_2 films with (XSE) and without (XSO) erbium as a function of annealing temperature, showing (a) the Er PL peak intensity (I_{Er}) and the decay time (τ_{Er}) at 1535 nm in XSE samples. (b) The PL intensities at 650 nm (I_{LC}^{XSE}) and 900 nm (I_{NC}^{XSE}) in XSE samples, the derived Er^{3+} excitation density in XSE samples (I_{Er}/τ_{Er}), the relative concentration of Er^{3+} ions coupled to sensitizers ($N_{Er,c}$), and the transfer efficiency at 650 nm derived from the spectral measurements ($\eta_{tr,PL}$). (c) The decay rate of the emission at 900 nm in XSO and XSE samples ($R_{dec,NC}^{XSO}$ and $R_{dec,NC}^{XSE}$, respectively), the derived transfer rate at 900 nm (R_{tr}), the excitation rate of the nanocrystals measured at 900 nm in XSO samples ($R_{exc,NC}^{XSO}$), the Er^{3+} excitation rate measured in XSE samples ($R_{exc,Er}$), the transfer efficiency at 900 nm derived from the lifetime measurements ($\eta_{tr,LT}$), and the transfer efficiency at 900 nm derived from spectral measurements ($\eta_{tr,PL,NC}$).

The Er^{3+} excitation density can be found from the Er^{3+} PL intensity and the Er^{3+} lifetime: assuming a constant Er^{3+} radiative emission rate, the Er^{3+} emission efficiency is known to be linearly proportional to the Er^{3+} lifetime. In the linear intensity vs pump power regime, the total Er^{3+} PL intensity is given by

$$I_{\mathrm{Er}} \propto R_{exc,\mathrm{Er}} \tau_{dec,\mathrm{Er}} N_{\mathrm{Er},c} = \tau_{dec,\mathrm{Er}} \rho_{exc,\mathrm{Er}}, \quad (1)$$

with $N_{\mathrm{Er},c}$ (cm^{-3}) the density of Er^{3+} ions that are coupled to a sensitizer and can be excited indirectly, $R_{exc,\mathrm{Er}}$ (s^{-1}) the Er^{3+} excitation rate, and $\tau_{dec,\mathrm{Er}}$ (s) the Er^{3+} lifetime. This shows that the Er^{3+} excitation density is proportional to $I_{\mathrm{Er}}/\tau_{dec,\mathrm{Er}}$. This quantity is included in Fig. 5(b) (solid triangles). Intriguingly, the Er^{3+} excitation density is found to follow the LC emission almost perfectly up to $T_{\mathrm{ann}} = 1000\ ^{\circ}\mathrm{C}$, after which it is found to drop steeply. The clear correlation of the Er^{3+} excitation density with the LC emission as well as the anticorrelation of the Er^{3+} excitation density with the NC PL intensity suggest that in these samples, LC-mediated Er^{3+} excitation dominates over NC-mediated Er^{3+} excitation.

Figure 5(c) shows the measured Er^{3+} excitation rate ($R_{\mathrm{Er},exc}$) as a function of annealing temperature. These values were obtained from the measured Er^{3+} rise times $\tau_{rise,\mathrm{Er}}$ and decay times $\tau_{dec,\mathrm{Er}}$ taken at 1535 nm, using the well known relation

$$R_{exc,\mathrm{Er}} = \frac{1}{\tau_{rise,\mathrm{Er}}} - \frac{1}{\tau_{dec,\mathrm{Er}}}. \quad (2)$$

The obtained values correspond to the *indirect* Er^{3+} excitation rate, since the excitation spectra in Fig. 4 showed no sign of direct Er^{3+} excitation, and no Er^{3+} PL was observed in EO samples when excited at 351 nm. The indirect Er^{3+} excitation rate is found to be remarkably independent of the annealing temperature, varying by less than 30% over the entire temperature range. This is a highly surprising result given the fact that in this same temperature range, the sample microstructure evolves dramatically from predominantly amorphous to clearly phase separated, as observed in the TEM analysis (Fig. 1). This observation leads us to conclude that the Er^{3+} excitation is due to a sensitizer whose nature does not change significantly for all annealing temperatures shown, *ruling out NC-mediated excitation as the predominant excitation mechanism*. Instead, it appears that the Er^{3+} excitation in these samples occurs predominantly via isolated excess-silicon-related luminescence centers.

The important role of LC-mediated Er^{3+} excitation is further confirmed by a calculation of the total concentration of Er^{3+} ions that are coupled to a sensitizer $N_{\mathrm{Er},c}$. This value can be derived from Eq. (1) in relative units based on the measured values of $R_{exc,\mathrm{Er}}$. The resulting $N_{\mathrm{Er},c}$ values have been included in Fig. 5(b) (solid gray line). The relative concentration of the indirectly excitable Er^{3+} is found to follow the LC emission almost perfectly up to 1000 °C, further supporting our conclusion that the Er^{3+} is predominantly excited via LCs in this temperature range. It should also be noted that the concentration of indirectly excitable Er^{3+} decreases by a factor of ~190 upon increasing T_{ann} from 600 to 1200 °C. This implies that the concentration of indirectly excited Er^{3+} in samples annealed at 1200 °C is as low as 0.63 at. %/190 = 3.3×10^{-3} at. %.

The sharp decrease of $N_{\mathrm{Er},c}$ at temperatures above 1000 °C at relatively constant excitation rate and relatively constant LC emission suggests that at annealing temperatures above 1000 °C, either Er^{3+} ions become optically inactive due to the onset of Er precipitation[51] or that the LC-mediated Er^{3+} excitation process is affected by the presence of Si nanocrystals. The latter theory seems to be supported by the rapid drop in the LC excited Er^{3+} emission at 981 nm for $T_{\mathrm{ann}} > 1000\ ^{\circ}\mathrm{C}$; however, further studies are needed to determine the exact origin of the reduced $N_{\mathrm{Er},c}$ at high annealing temperatures.

D. Evidence for nanocrystal-mediated excitation

Although the previous discussion demonstrates that LC-mediated Er^{3+} excitation *dominates* in these measurements, the reduction of the NC PL upon Er^{3+} incorporation suggests that a finite amount of NC-mediated Er^{3+} excitation occurs in these samples as well. To learn about the efficiency of this parallel process, lifetime measurements were performed on XSE and XSO samples annealed at 1000, 1100, and 1200 °C, all of which exhibited clear NC luminescence. These decay traces were measured at an emission wavelength of 900 nm to minimize the PL contribution from the LC band and to ensure that the photoluminescence measurements represent a fixed nanocrystal size. The measured decay traces exhibited multiexponential decay with dispersion factors β between 0.5 and 0.8 for samples annealed at temperatures between 1000 and 1200 °C. The corresponding $1/e$ decay rates have been included in Fig. 5(c). The NC decay rate of the XSO samples ($R^{XSO}_{dec,NC}$, solid circles) is seen to decrease approximately by a factor of 12 as T_{ann} increases from 1000 to 1200 °C. This type of decay rate decrease with increasing T_{ann} is commonly attributed to an increasingly indirect band gap as the NC diameter increases.[52] Comparing these decay rates with those observed in XSE samples ($R^{XSE}_{dec,NC}$, open circles), an increase in the total decay rate by a factor ~3–4 is observed for each of these temperatures, suggesting the introduction of an additional nonradiative exciton recombination path due to the presence of Er^{3+} ions. This strongly suggests that despite the fact that most of the observed Er^{3+} PL is due to LC-mediated excitation, Si nanocrystals *do* participate in Er^{3+} excitation in these samples. The Er induced difference in nanocrystal lifetime provides further information about the nature of the nanocrystal-mediated excitation process. Based on the measured decay rates, it is possible to determine the total NC energy transfer rate $R_{tr} = 1/\tau_{tr}$. Here, τ_{tr} is the total transfer time, which we define as the time required for an exciton confined in a silicon NC to recombine nonradiatively, exciting a nearby Er^{3+} ion. The total NC decay rate in the presence of Er^{3+} is then given by

$$\frac{1}{\tau^{XSE}_{dec,NC}} = \frac{1}{\tau^{XSO}_{dec,NC}} + R_{tr}, \quad (3)$$

where $\tau^{XSE}_{dec,NC}$ and $\tau^{XSO}_{dec,NC}$ are the measured $1/e$ lifetimes of the nanocrystal PL at 900 nm. Note that this relation assumes that all additional nonradiative decay observed in the XSE sample is due to energy transfer. The resulting total transfer rate (R_{tr}) has been included in Fig. 5(c) (crossed circles). The total transfer rate is found to decrease by more than an order of magnitude as T_{ann} is increased from 1000 to 1200 °C, and is found to be approximately proportional to the NC rate of

the XSO sample. These findings seem to suggest that the NC-to-Er^{3+} transfer rate depends on the oscillator strength of the exciton recombination in Si nanocrystals as one would expect for a Förster-type energy transfer. Note that in order to fully demonstrate the correlation between the oscillator strength and the transfer rate, the nanocrystal radiative rate should be determined independently.

Based on the measured NC lifetime (LT) data, the quantum efficiency of the nanocrystal-mediated energy transfer can be found using

$$\eta_{tr,LT} = \frac{R_{tr}}{R_{dec,NC}^{XSE}} = \frac{\tau_{dec,NC}^{XSE}}{\tau_{tr}}, \tag{4}$$

where we have again assumed that all nonradiative decay introduced by the Er^{3+} ions is related to energy transfer events. The thus obtained transfer efficiency is shown in Fig. 5(c) ($\eta_{tr,LT}$, crosses). Note that the nanocrystal-mediated transfer efficiency is in the range of 60%–75%, in agreement with earlier efficiency estimates.[26]

For comparison, we have also determined the energy transfer quantum efficiency based on the photoluminescence spectra shown in Fig. 2. In the following, we briefly describe how this can be done without explicit knowledge of PL lifetimes. For a fixed pump power in the linear pump regime using a fixed excitation and collection geometry, the collected signal intensity for the XSO sample at a given emission wavelength is proportional to

$$I_i^{XSO} \propto \sigma_{abs,i} N_i \frac{R_{rad,i}}{R_{rad,i} + R_{nr,i}}, \tag{5}$$

where i represents the type of sensitizer (LC or nanocrystals), $\sigma_{abs,i}$ is the corresponding absorption cross section, N_i is the corresponding volume density of these sensitizers, and $R_{rad,i}$ and $R_{nr,i}$ are the radiative and nonradiative recombination rates for the corresponding sensitizer. As discussed above, the addition of Er^{3+} ions is assumed to lead to the introduction of an additional nonradiative decay process at a rate R_{tr}. The intensity observed from an XSE sample is reduced due to this additional decay, and is given by

$$I_i^{XSE} \propto \sigma_{abs,i} N_i \frac{R_{rad,i}}{R_{rad,i} + R_{nr,i} + R_{tr}}, \tag{6}$$

Assuming that the presence of Er^{3+} does not affect the density or the absorption cross section of the sensitizer, we can use these measured PL intensities to derive the transfer efficiency as follows:

$$\begin{aligned} \eta_{tr,i,PL} &= \frac{R_{tr}}{R_{rad,i} + R_{nr,i} + R_{tr}} \\ &= \frac{(R_{rad,i} + R_{nr,i} + R_{tr}) - (R_{rad,i} + R_{nr,i})}{R_{rad,i} + R_{nr,i} + R_{tr}} \\ &= 1 - \frac{I_i^{XSE}}{I_i^{XSO}}. \end{aligned} \tag{7}$$

Based on this equation, we can obtain a value for the transfer efficiency as a function of emission wavelength. The results have been included in Fig. 2 for samples annealed at 600 °C (dotted line) and 1100 °C (dashed line). Note that results for $\lambda_{em} > 940$ nm are not included in the graph since the formulas used do not take into account the appearance of the observed Er^{3+}-related emission at this wavelength. The PL based transfer efficiency is found to be >80% throughout the entire spectral range, confirming that both LCs and NCs can efficiently excite Er^{3+}. Surprisingly, the transfer efficiency is found to be approximately constant across the emission spectrum of the LCs and the NCs, implying that the obtained efficiency value at a fixed wavelength can be taken to represent the total transfer efficiency. The values for the energy transfer efficiency based on the PL intensities at $\lambda_{em} = 650$ nm, corresponding to predominantly LC-mediated excitation, have been included in Fig. 5(b) (stars). The values for $\lambda_{em} = 900$ nm, corresponding to predominantly NC-mediated Er excitation at $T_{ann} \geqslant 1000$ °C, have been included in Fig. 5(c) (plus symbols). Using this method, the NC-mediated transfer efficiency at $T_{ann} = 1100$ °C is found to be 84%, in reasonable agreement with the value of 70% that was obtained using the lifetime analysis described above. We attribute the discrepancy to the fact that $1/e$ lifetimes were used in the analysis, which does not take into account the multiexponential nature of the nanocrystal PL decay traces.

A final point that needs to be addressed is the effective Er^{3+} absorption cross section. In previous studies, the similarity between the magnitude of the indirect Er^{3+} absorption cross section and the measured Si nanocrystal absorption cross section seemed to indicate that the NC excitation and the Er^{3+} excitation had the same origin. However, from the constant Er^{3+} excitation rate in Fig. 5(c), it is clear that the same effective absorption cross section is observed at all annealing temperatures, even well below the temperatures needed for nanocrystal formation. From the excitation rate data and the known pump power, the LC-mediated effective Er^{3+} excitation cross section at an excitation wavelength of $\lambda_{exc} = 351$ nm is $\sigma_{Er,LC}(351\ \text{nm}) \approx 2 \times 10^{-14}\ \text{cm}^2$. To compare the results of the present samples with previous studies, we also measured the nanocrystal excitation rate for XSO samples annealed at T_{ann} between 1000 and 1200 °C based on the emission at 900 nm and the well known relation

$$R_{exc,NC}^{XSO} = R_{rise,NC}^{XSO} - R_{dec,NC}^{XSO}. \tag{8}$$

The resulting nanocrystal excitation rate has been included in Fig. 5(c) (solid triangles). For these three temperatures, the nanocrystal excitation rate is found to be $5700 \pm 900\ \text{s}^{-1}$. Based on the measured excitation rate, the nanocrystal absorption cross section at 351 nm is calculated to be $\sigma_{NC}(351\ \text{nm}) \approx 5 \times 10^{-14}\ \text{cm}^2$, in good agreement with the literature.[13] Comparing these results with the Er^{3+} excitation rate determined above, we find that the effective Er^{3+} absorption cross section is approximately constant and a factor ~2.5 lower than the nanocrystal absorption cross section, similar to the results obtained in previous studies.[16,26] However, in contrast with previous studies, this Er^{3+} excitation rate does not necessarily indicate nanocrystal-mediated excitation, but, instead, is due to a combination of LC- and NC-mediated excitations.

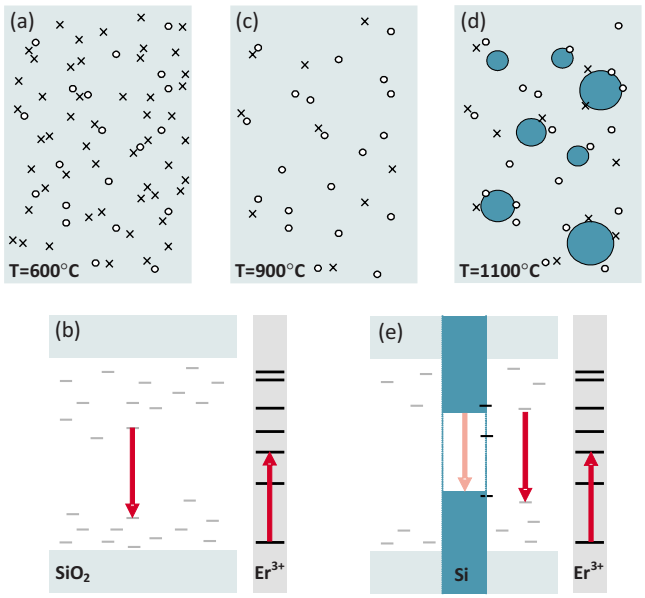

FIG. 6. (Color online) Schematic representation of the Er^{3+} excitation processes in Er-doped Si-rich SiO_2 samples (a) at low annealing temperatures, showing a high concentration of excess-Si-related LCs indicated by crosses, as well as Er^{3+} ions, indicated by open circles, and (b) the corresponding schematic band diagram, indicating the SiO_2 valence band and conduction band, LC-related electronic levels in the band gap indicated by the horizontal lines, as well as the Er^{3+} energy levels (LC-mediated excitation is indicated by the vertical arrows); (c) at intermediate annealing temperatures, showing a reduced concentration of LCs; and (d) at high annealing temperatures, showing the formation of Si nanocrystals (dark circles), and (e) the corresponding band diagram, indicating the presence of Si nanocrystals with a quantum confined band gap. A weak exciton-mediated contribution to the Er excitation is indicated by the light vertical arrow.

E. Discussion

Based on the experimental observations presented in this paper, we have arrived at the physical model shown in Fig. 6. At low annealing temperatures, the SiO_2 film contains Er^{3+} ions and a high concentration of luminescence centers, as indicated schematically in Fig. 6(a). Figure 6(b) shows the corresponding band diagram, with LC-related levels in the SiO_2 band gap indicated by horizontal gray lines. After optical excitation of a electron into a LC-related level, electronic relaxation from this level (downward arrow) to a lower lying level leads to the observed indirect Er^{3+} excitation (upward arrow) with a time constant substantially faster than 80 ns. Note that the sketch indicates Er^{3+} excitation into the $^4I_{11/2}$ level; however, the fraction of excitation into the $^4I_{11/2}$ level, the $^4I_{13/2}$ level, and possibly other Er^{3+} levels cannot be determined from the present data. At higher annealing temperatures but before the onset of nanocluster formation, the density of LCs is reduced substantially [Fig. 6(c)], leading to a reduced number of excitable Er^{3+} ions and a reduced PL intensity, but exhibiting an unmodified indirect Er^{3+} excitation cross section. At temperatures above the onset of nanocluster formation, the density of LCs continues to decrease, while the formation of Si nanocrystals could lead to the generation of similar electronic states at the nanocrystal surface [Fig. 6(d)]. The corresponding band diagram is shown in Fig. 6(e). Despite the presence of Si nanocrystals, LC-mediated excitation (dark downward arrow) continues to dominate over nanocrystal-mediated excitation (light downward arrow). Note that the ratio between these processes most likely depends on the excitation wavelength, which is not explicitly investigated here.

The observations described above have several implications for the interpretation of data already present in the literature. First, a dominant LC-mediated excitation mechanism could resolve a long standing controversy: in measurements of the indirect Er^{3+} excitation rate as a function of Er^{3+} concentration, it was observed that the Er^{3+} excitation rate remained approximately constant as the Er^{3+} concentration was increased by more than an order of magnitude.[16] It was therefore concluded that Si NCs can excite only 1–2 Er atoms. In light of our observations, it seems likely that in those measurements, a single sensitizer, indeed, could excite no more than 1–2 Er^{3+} ions. However, the observed sensitization may not have been directly caused by Si nanocrystals, but rather by isolated LCs, resulting in an Er^{3+} excitation rate approximately independent of the Er^{3+} concentration. Due to the "atomic" size scale that such LCs could have, the limitation of 1–2 Er ions per LC would seem physically reasonable. Second, the presence of a dominant LC-mediated Er^{3+} excitation process could, in part, explain the experimentally observed independent behavior of the nanocrystal PL and the Er^{3+} PL as a function of sample temperature in the temperature range of 20–300 K.[26,29] In these studies, the nanocrystal lifetime and intensity were found to vary significantly as a function of temperature, while the Er^{3+} PL intensity remained approximately constant. A fast exciton-Er^{3+} energy transfer process was assumed to be responsible for this behavior, rendering nanocrystals coupled to Er^{3+} inefficient ("dark"). Although the existence of relatively dark nanocrystals is confirmed by the PL spectra observed in this study, it now seems likely that part of the insensitivity of the Er^{3+} PL to the sample temperature observed in literature is related to the existence of a significant fraction of LC-mediated Er^{3+} excitation. Third, our observations show that two distinct transfer processes are present with a fast process ($\tau_{tr} < 80$ ns) dominant over a slow process ($\tau_{tr} \sim 4-100$ μs), which is in good agreement with the findings of Fujii *et al.*,[24] who also observed that two energy transfer processes exist: a fast process ($\tau_{tr} < 100$ ns) and a slow process ($\tau_{tr} \sim 1-70$ μs), with the fast process always dominant. This was explained in a later publication by Imakita *et al.*[25] by assuming that the energy transfer mechanism depends on the distance of the Er^{3+} ions from the nanocrystal surface. Note that this model does not predict the existence of a fast transfer process at temperatures below the onset of nanocrystal formation, nor the observation of an annealing temperature independent Er^{3+} excitation rate. In light of the present results, it appears that the observed fast transfer in those studies may also have been associated with Er^{3+} sensitization by discrete luminescence centers in the oxide, while the slow transfer process, indeed, was related to the known and efficient (but less prevalent) energy transfer via excitons confined in Si nanocrystals.

Our interpretation of the present data does not seem to conflict with existing data in literature and resolves some outstanding controversies; however, a remaining intriguing coincidence should be pointed out. As mentioned earlier, the effective LC-mediated Er^{3+} cross section under excitation with 351 nm light was estimated to be of the order of 2×10^{-14} cm^2. In our present interpretation, this value represents the LC absorption cross section, multiplied by the near unity transfer efficiency. Coincidentally, the absorption cross section associated with the NC emission as found from lifetime measurements in the present study is found to be of a very similar magnitude, given by $\sigma_{NC} \approx 5 \times 10^{-14}$ cm^2, corresponding very well with values found in the literature.[13] A similar absorption cross section for these apparently entirely different physical entities (an isolated electronic state vs a collection of $\sim 10^3$ atoms) seems surprising, and suggests that a direct physical link may exist between the LC and NC emissions. A tempting explanation is that the observed LC PL is mediated by Si nanocrystal excitation; however, since this model requires the existence of Si nanocrystals, it cannot explain the observation of a constant Er^{3+} absorption cross section as a function of annealing temperature. An alternate explanation is that Si nanocrystals are excited via LCs, resulting in a similar absorption cross section and a similar excitation spectrum for both PL features. The latter possibility would also explain the approximately constant NC absorption cross section for the three highest annealing temperatures (1000, 1100, and 1200 °C). Finally, it could partly explain the strong overall reduction of the NC photoluminescence spectrum without the introduction of clear dips in the NC emission spectra at emission energies resonant with Er^{3+} transition energies, since the energy transfer from LCs to Er^{3+} would compete with the energy transfer from LCs to Si nanocrystals. Note that this explanation only involves the *excitation* mechanism for the NC emission band, i.e., it does allow for this emission to be caused by quantum confined excitons, as convincingly demonstrated by many studies in the literature. Despite matching several experimental observations, it is not clear how such a LC-mediated NC excitation process could dominate over the direct Si nanocrystal excitation, which, based on a typical nanocrystal diameter between 3 and 10 nm and the known bulk Si absorption coefficient, can be estimated to be of the order of 10^{-14}–10^{-12} cm^2 at $\lambda_{exc}=351$ nm.

The observations made in this study could have a major impact on the maximum gain that can be achieved in Si-sensitized Er^{3+} based waveguide amplifiers. As mentioned in the Introduction, confined carrier absorption is considered to be a severe challenge in Si-nanocrystal-sensitized systems due to the relatively long exciton lifetime and large anticipated confined carrier absorption cross section at 1.53 μm compared to the small Er^{3+} emission cross section at that same wavelength.[1,20,53–55] It is now clear that fast ($\tau_{tr} < 80$ ns) indirect Er^{3+} excitation can occur in these materials *without the presence of Si nanocrystals*, and therefore, without the presence of long lived excitons, while retaining the large effective Er^{3+} excitation cross sections observed in literature. Also, the concentration of indirectly excitable Er^{3+} ions $N_{Er,c}$ obtained at low annealing temperatures is shown to be a factor of 10–100 higher than that obtained at the annealing temperatures required to form nanocrystals. Since the optical gain coefficient scales linearly with the Er^{3+} concentration, our results suggest that maximum gain can be achieved at low processing temperatures, albeit with a reduced Er^{3+} emission quantum efficiency associated with the relatively short Er^{3+} lifetime.

IV. CONCLUSIONS

The indirect excitation of Er^{3+} ions in Er-doped Si-rich SiO_2 samples annealed at temperatures in the range of 600–1200 °C has been investigated. It was demonstrated that the dominant indirect excitation mechanism involves fast ($\tau_{tr} < 80$ ns) Er^{3+} excitation by isolated LCs at all annealing temperatures, while for annealing temperatures exceeding ~1000 °C, a small fraction of the Er^{3+} excitation events is mediated by exciton recombination in Si nanocrystals, with a typical transfer time in the range of 4–100 μs. Both excitation processes were found to exhibit a transfer efficiency $\geqslant 60\%$. The LC-mediated indirect Er^{3+} excitation cross section at an excitation wavelength of 351 nm was found to be independent of annealing temperature with a magnitude of 2×10^{-14} cm^2, while the nanocrystal absorption cross section at the same wavelength was found to be 5×10^{-14} cm^2. The proposed interpretation of the measurements was shown to explain several observations in the literature. A maximum concentration of indirectly excitable Er^{3+} was found at the lowest annealing temperature used (600 °C), suggesting that Er-doped optical amplification media in Si-sensitized SiO_2 hosts will exhibit maximum gain for processing temperatures well below those required for the onset of nanocrystal formation.

ACKNOWLEDGMENTS

This work was supported by the DARPA EPIC program (Contract No. 67SA-1072809) and by the National Science Foundation (CAREER No. ECCS-0644228).

*Corresponding author; osavchyn@mail.ucf.edu

†Also at Physics Department, University of Central Florida, 4000 Central Florida Blvd., Orlando, FL 32816.

‡Also at School of Electrical Engineering and Computer Science, University of Central Florida, 4000 Central Florida Blvd., Orlando, FL 32816.

§Present address: Semiconductor Research and Development Center, IBM Microelectronics, 2070 Route 52, Hopewell Junction, NY 12533.

‖Also at Department of Mechanical, Materials and Aerospace Engineering, University of Central Florida, 4000 Central Florida Blvd., Orlando, FL 32816.

[1] P. G. Kik and A. Polman, in *Proceedings of the NATO Advanced Research Workshop on Towards the First Silicon Laser, Trento,*

Italy, 2002, edited by L. Pavesi, S. Gaponenko, and L. Dal Negro (Kluwer Academic, Dordrecht, 2003), p. 383.
[2] M. Lipson, J. Lightwave Technol. **23**, 4222 (2005).
[3] T. J. Kippenberg, J. Kalkman, A. Polman, and K. J. Vahala, Phys. Rev. A **74**, 051802(R) (2006).
[4] A. Polman, B. Min, J. Kalkman, T. J. Kippenberg, and K. J. Vahala, Appl. Phys. Lett. **84**, 1037 (2004).
[5] A. J. Kenyon, Semicond. Sci. Technol. **20**, R65 (2005).
[6] N. Daldosso, D. Navarro-Urrios, M. Melchiorri, C. García, P. Pellegrino, B. Garrido, C. Sada, G. Battaglin, F. Gourbilleau, R. Rizk, and L. Pavesi, IEEE J. Sel. Top. Quantum Electron. **12**, 1607 (2006).
[7] L. Dal Negro, J. H. Yi, J. Michel, L. C. Kimerling, S. Hamel, A. Williamson, and G. Galli, IEEE J. Sel. Top. Quantum Electron. **12**, 1628 (2006).
[8] W. Miniscalco, in *Rare-Earth-Doped Fiber Lasers and Amplifiers*, edited by M. Digonnet (Dekker, New York, 2001), p. 62.
[9] A. Polman and F. C. J. M. van Veggel, J. Opt. Soc. Am. B **21**, 871 (2004).
[10] T. Kimura, A. Yokoi, H. Horiguchi, R. Saito, T. Ikoma, and A. Sato, Appl. Phys. Lett. **65**, 983 (1994).
[11] G. N. van den Hoven, Jung H. Shin, A. Polman, S. Lombardo, and S. U. Campisano, J. Appl. Phys. **78**, 2642 (1995).
[12] M. Fujii, M. Yoshida, Y. Kanzawa, S. Hayashi, and K. Yamamoto, Appl. Phys. Lett. **71**, 1198 (1997).
[13] D. Kovalev, J. Diener, H. Heckler, G. Polisski, N. Künzner, and F. Koch, Phys. Rev. B **61**, 4485 (2000).
[14] G. Franzó, V. Vinciguerra, and F. Priolo, Appl. Phys. A: Mater. Sci. Process. **69**, 3 (1999).
[15] F. Gourbilleau, M. Levalois, C. Dufour, J. Vicens, and R. Rizk, J. Appl. Phys. **95**, 3717 (2004).
[16] P. G. Kik and A. Polman, J. Appl. Phys. **88**, 1992 (2000).
[17] A. J. Kenyon, C. E. Chryssou, C. W. Pitt, T. Shimizu-Iwayama, D. E. Hole, N. Sharma, and C. J. Humphreys, J. Appl. Phys. **91**, 367 (2002).
[18] M. Wojdak, M. Klik, M. Forcales, O. B. Gusev, T. Gregorkiewicz, D. Pacifici, G. Franzó, F. Priolo, and F. Iacona, Phys. Rev. B **69**, 233315 (2004).
[19] J. Lee, J. H. Shin, and N. Park, J. Lightwave Technol. **23**, 19 (2005).
[20] P. G. Kik and A. Polman, J. Appl. Phys. **91**, 534 (2002).
[21] N. Daldosso, D. Navarro-Urrios, M. Melchiorri, L. Pavesi, F. Gourbilleau, M. Carrada, R. Rizk, C. García, P. Pellegrino, B. Garrido, and L. Cognolato, Appl. Phys. Lett. **86**, 261103 (2005).
[22] D. Pacifici, G. Franzó, F. Priolo, F. Iacona, and L. Dal Negro, Phys. Rev. B **67**, 245301 (2003).
[23] A. Mimura, M. Fujii, S. Hayashi, D. Kovalev, and F. Koch, Phys. Rev. B **62**, 12625 (2000).
[24] M. Fujii, K. Imakita, K. Watanabe, and S. Hayashi, J. Appl. Phys. **95**, 272 (2004).
[25] K. Imakita, M. Fujii, and S. Hayashi, Eur. Phys. J. D **34**, 161 (2005).
[26] P. G. Kik, M. L. Brongersma, and A. Polman, Appl. Phys. Lett. **76**, 2325 (2000).
[27] K. Imakita, M. Fujii, and S. Hayashi, Phys. Rev. B **71**, 193301 (2005).
[28] K. Watanabe, M. Fujii, and S. Hayashi, J. Appl. Phys. **90**, 4761 (2001).
[29] M. Fujii, M. Yoshida, S. Hayashi, and K. Yamamoto, J. Appl. Phys. **84**, 4525 (1998).
[30] G. Franzó, S. Boninelli, D. Pacifici, F. Priolo, F. Iacona, and C. Bongiorno, Appl. Phys. Lett. **82**, 3871 (2003).
[31] F. Gourbilleau, R. Madelon, C. Dufour, and R. Rizk, Opt. Mater. (Amsterdam, Neth.) **27**, 868 (2005).
[32] F. Enrichi, G. Mattei, C. Sada, E. Trave, D. Pacifici, G. Franzò, F. Priolo, F. Iacona, M. Prassas, M. Falconieri, and E. Borsella, Opt. Mater. (Amsterdam, Neth.) **27**, 904 (2005).
[33] L.-F. Bian, C. G. Zhang, W. D. Chen, C. C. Hsu, and Tongfei Shi, Appl. Phys. Lett. **89**, 231927 (2006).
[34] J. S. Chang, J.-H. Jhe, M.-S. Yang, J. H. Shin, and K. J. Kim, and D. W. Moon, Appl. Phys. Lett. **89**, 181909 (2006).
[35] C. Y. Chen, W. D. Chen, S. F. Song, Z. J. Xu, X. B. Liao, G. H. Li, and K. Ding, J. Appl. Phys. **94**, 5599 (2003).
[36] A. Hryciw, C. Blois, A. Meldrum, T. Clement, R. DeCorby, and Quan Li, Opt. Mater. (Amsterdam, Neth.) **28**, 873 (2006).
[37] http://www.genplot.com/
[38] F. Iacona, C. Bongiorno, C. Spinella, S. Boninelli, and F. Priolo, J. Appl. Phys. **95**, 3723 (2004).
[39] T. Shimizu-Iwayama, K. Fujita, S. Nakao, K. Saitoh, T. Fujita, and N. Itoh, J. Appl. Phys. **75**, 7779 (1994).
[40] M. Ya. Valakh, V. A. Yukhimchuk, V. Ya. Bratus, A. A. Konchits, P. L. F. Hemment, and T. Komoda, J. Appl. Phys. **85**, 168 (1999).
[41] J.-Y. Zhang, X.-M. Bao, N.-S. Li, and H.-Z. Song, J. Appl. Phys. **83**, 3609 (1998).
[42] A. J. Kenyon, P. F. Trwoga, C. W. Pitt, and G. Rehm, J. Appl. Phys. **79**, 9291 (1996).
[43] K. S. Min, K. V. Shcheglov, C. M. Yang, Harry A. Atwater, M. L. Brongersma, and A. Polman, Appl. Phys. Lett. **69**, 2033 (1996).
[44] I. N. Yassievich and A. S. Moskalenko, Mater. Sci. Eng., B **105**, 192 (2003).
[45] J. S. Biteen, N. S. Lewis, H. A. Atwater, and A. Polman, Appl. Phys. Lett. **84**, 5389 (2004).
[46] M. L. Brongersma, P. G. Kik, A. Polman, K. S. Min, and H. A. Atwater, Appl. Phys. Lett. **76**, 351 (2000).
[47] M. V. Wolkin, J. Jorne, P. M. Fauchet, G. Allan, and C. Delerue, Phys. Rev. Lett.. **82**, 197 (1999).
[48] G. H. Dieke and H. M. Crosswhite, Appl. Opt. **2**, 675 (1963).
[49] P. W. France, M. G. Drexhange, J. M. Parker, M. W. Moore, S. F. Carter, and J. V. Wright, *Fluoride Glass Optical Fibres* (Balckie, Boca Raton, FL, 2000), p. 167.
[50] A. Polman, D. C. Jacobson, A. Lidgard, J. M. Poate, and G. W. Arnold, Nucl. Instrum. Methods Phys. Res. B **59-60**, 1313 (1991).
[51] A. Polman, D. C. Jacobson, D. J. Eaglesham, R. C. Kistler, and J. M. Poate, J. Appl. Phys. **70**, 3778 (1991).
[52] D. Kovalev, H. Heckler, G. Polisski, J. Diener, and F. Koch, Opt. Mater. (Amsterdam, Neth.) **17**, 35 (2001).
[53] W. Miniscalco, J. Lightwave Technol. **9**, 234 (1991).
[54] H. Mertens, A. Polman, I. M. P. Aarts, W. M. M. Kessels, and M. C. M. van de Sanden, Appl. Phys. Lett. **86**, 241109 (2005).
[55] H.-S. Han, S.-Y. Seo, J. H. Shin, and N. Park, Appl. Phys. Lett. **81**, 3720 (2002).